Composites Part C: Open Access 5 (2021) 100151

Contents lists available at ScienceDirect

Composites Part C: Open Access

journal homepage: www.elsevier.com/locate/jcomc

Fiber misalignment analysis in PCM-UD composite materials by Full Field Nodal Method

Luca Raimondi[a,*], Tommaso Maria Brugo[a,b], Andrea Zucchelli[a,b,**]

[a] DIN – Università di Bologna, Viale Risorgimento 2, 40136 Bologna, Italia
[b] CIRI-MAM – Università di Bologna, Viale Risorgimento 2, 40136 Bologna, Italia

ARTICLE INFO

Keywords:
Fabrics/textiles
Defects
Elastic properties
Finite Element Analysis (FEA)
Non-destructive testing
Optical microscopy
FFNM

ABSTRACT

In this work, a new full-field and non-destructive methodology for measuring process-induced fiber waviness in composites are presented, benchmarked, and successfully applied to predict long fiber-reinforced stiffness composite laminates. The proposed method, named the "Full Field Nodal Method" (FFNM), computes the misalignment angle by interpolating the displacement measured on a discrete set of sampling points. Sampling points have been traced on the prepreg surface before curing, and bilinear Lagrangian interpolating functions have been adopted and compared. Several samples, made with compression molded prepreg, have been used to test the new method capabilities in this work. A first benchmark was done measuring the fiber waviness on samples through the new method and by another one recently presented in the literature. Average fiber angles predicted by the FFNM, with bilinear interpolating functions, were in high agreement with experimental results. Fiber angle misalignment measured by FFNM was used to orientate the reference system of elements of the FEA model. Numerical results in terms of stiffness and strain field were compared to those detected by the Digital Image Correlation technique (DIC) during the tensile tests. Comparison of numerical and experimental results showed an excellent prediction of material stiffness and the strain field with an error of 15%.

1. Introduction

Recent advances in polymers and novel out-of-autoclave techniques have enabled composite materials to be at the forefront of lightweight technologies in the automotive and transportation industries [1]. Long fiber carbon prepregs have been traditionally formulated for autoclave processing, but continuous improvement in fast-curing resins has recently extended their processability to compression molding, enabling this technology suitable for high volume part production [2]. Despite its attractive benefits, prepreg compression molding (PCM) can produce more significant fiber misalignment to the autoclave process, especially when continuous fibers are co-molded with discontinuous fibers [3,4]. It is worth mentioning that prepreg is subjected to an intense flow during PCM processing favored by the system's high heat efficiency, the limited heat capacity of small thickness prepreg charge, and the tools' high compressing speed. Rheological studies in long discontinuous fibers composites [5–7] have demonstrated that the effective viscosity tensor is highly anisotropic with maximum elongational viscosity in the fiber direction. Sommer [8] reports that compression molding with long fiber composites is aptly described by a plug flow with highly anisotropic in-plane behavior. According to the cited literature, it can be argued that fiber waviness in a PCM process is caused by fiber transport and interaction phenomena correlated to the flow characteristics in the mold. The negative effect of fiber misalignment on composites under compressive loading has been widely studied [9,10], and homogenization techniques have been proposed [11]. The issues related to the previously cited literature highlight the need to identify practical tools that have to quantify fiber misalignment in composite materials as a result of the process to predict the mechanical properties of the components. Several techniques have been developed to measure and detect fiber distortion, mostly based on 2D micrography. Yurgartis [12] proposed a method based on the measurement of the fibers' ellipticity in a cross-section of the component. By measuring the major and minor axes of the ellipsoids and knowing the fiber diameter, the 3D spatial orientation of the fibers can be estimated. This method, however, is destructive and it is not able to identify the sign (positive or negative) of the deviation of the fibers and is more limited by the fact that the cross-section of the fibers is not always perfectly circular. Kratmann and others [13] and, more recently, Wilhelmsson and Asp [14] settled methodologies in which surfaces parallel to fiber direction were sand gridded and evaluated by image algorithm on a 2D micrograph. The methods have been proven to be robust and economical, however require sample preparation that irreversibly damages the surface of the composite.

* Corresponding author.
** Corresponding author at: CIRI-MAM – Università di Bologna, Viale Risorgimento 2, 40136 Bologna, Italia.
E-mail addresses: luca.raimondi@unibo.it (L. Raimondi), a.zucchelli@unibo.it (A. Zucchelli).

https://doi.org/10.1016/j.jcomc.2021.100151
Received 27 February 2021; Received in revised form 26 April 2021; Accepted 4 May 2021

Recently, some Non-destructive testing (NDT) methodologies were proposed to detect fiber misalignment using Micro Computed Tomography (micro-CT) [15] or eddy current [16]. However, these techniques are challenging to be implemented in a mass production line to perform a real-time quality inspection. From the state of the art analysis, it is clear that most current methods for determining the fiber orientations in a composite part require expensive equipment, are difficult to perform on full-sized parts, or result in the part being destroyed. This work aims to settle a fast and cost-effective methodology for estimating in-plane fiber misalignment in molded composite components by analyzing the displacement field that occurs on a discrete number of points on the surface of the part during the manufacturing process. The precision of the proposed method, namely Full Field Nodal Method (FFNM), is successfully benchmarked with one of the most recent methodologies available in the state of the art, and potential advantages of implementation in FEA analysis for stiffness prediction is demonstrated. The proposed NDT, being a fast, full field optical technique, can be easily implemented in real time process monitoring either for stiffness and strength prediction of UD PCM components, either for assessing process parameters to reduce fiber misalignment defects.

2. Materials and methods

Materials and plate manufacturing are described in Section 2.1, the step-by-step description of the FFNM procedure is explained in Section 2.2 and experimental validation methods are illustrated in Section 2.3.

2.1. Materials and plates manufacturing

Prepreg used in the study was a UD P 384_S supplied by Torayca, Tokyo, Japan. This material is manufactured with T700S high strength carbon fibers and impregnated with 40% (V_f) #2300 resin, both manufactured by Toray Industries. This prepreg's initial misalignment angle was measured to be 0.88°, as reported in Supplementary Data, Section S2. A total of 3 plates (1 for optical microscopy analysis and 2 for both mechanical testing and optical microscopy analysis) were manufactured by stacking 3 plies of UD P 384_S4 in the $[0^\circ]_3$ configuration. The preassembled plies were grided according to the procedure described in next Section 2.2 and compression-molded. To ensure demoldability, the release agent employed was a Chemlease® PMR EZ supplied by ChemTrend L.P. Howell, Michigan United States.

2.2. Step-by-step description of the proposed methodology

The proposed method can be described in 3 main steps: preparation of the surface and subsequent compression molding (Section 2.2.1), digitalization, image processing and corners detection (Section 2.2.2), deformation analysis and fiber misalignment detection (Section 2.2.3).

2.2.1. Step 1: surface sampling points preparation and compression molding

In the present work, sampling points were generated as corners of a uniform, equally spaced, 35 mm grid. In particular, the grid has been drawn in two perpendicular directions directly on the wet prepreg by using a 3 mm wide Berner paint marker, with a similar approach to the one described in [3]. Before the curing phase, samples were scanned into a Kyocera TASKalfa 3501i Multifunction Laser Printer with a resolution of 600 × 600 dpi. After that, the 3 gridded prepreg plates were compression molded into a 320 × 320 mm tool designed to produce arbitrary thickness plates and installed in a downstroke AEM3 press. The temperature of the tool was set at 140 °C and monitored by 2 thermocouples. The tool was spray-coated with the release agent, the charge was 98% tool coverage, and plates were manufactured using a 15 min cycle at 56.4 bar pressure. After curing, samples were extracted, cooled in free air up to room temperature, and scanned with the previously mentioned equipment at the same resolution of 600 × 600 dpi.

2.2.2. Step 2: image processing and corners location detection

Scanned images were processed using custom software written in Matlab R2019a. The script performs a series of image manipulation and cleaning techniques to remove the noise and detect each corner's coordinate location. The step-by-step procedure is reported in Supplementary Data, Section S1.

2.2.3. Step 3: deformation analysis and Fiber Misalignment detection

The displacement of sample points of the grid, identified as the difference $\bar{\boldsymbol{u}}$ of their position prior and after compression molding by the procedure described in Section 2.2.2, were considered as nodal displacements of a set of 4 nodes interconnected iso-parametric elements. For each element, according to the formulation described in [17,18], both components of the displacement field and position were approximated using interpolating "shape" functions N_i, so that $\boldsymbol{u} = \sum_{i=1}^{4} N_i u_i, \boldsymbol{v} = \sum_{i=1}^{4} N_i v_i$ and $\boldsymbol{x} = \sum_{i=1}^{4} N_i x_i$, $\boldsymbol{y} = \sum_{i=1}^{4} N_i y_i$, being u_i and v_i the displacement component in x and y directions of element nodes, $\boldsymbol{u,v}$, and $\boldsymbol{x, y}$ respectively, the components of the displacement field $\boldsymbol{U}$ and the components of the position vector $\boldsymbol{X}$ in the image reference system for each element of the grid as shown in Fig. 1 a and b. This approach [19] allows calculating the in-plane components of the element deformation by its gradient $\boldsymbol{F_{el}}$, as a function of nodal displacement $\bar{\boldsymbol{u}}$ and shape functions by the relationship

$$\boldsymbol{F}_{el} = \boldsymbol{I} + \sum_{j=1}^{n} \bar{\boldsymbol{u}}^j \otimes \frac{\partial N^j}{\partial \boldsymbol{X}} \tag{1}$$

where $\boldsymbol{I}$ is the identity matrix. Both deformation and rigid body rotation are combined in the operator mentioned above: separation of the two has been conducted by considering the transformation $\boldsymbol{F}_{el} = \frac{1}{2}(\boldsymbol{F}_{el} + \boldsymbol{F}_{el}^T) + \frac{1}{2}(\boldsymbol{F}_{el} - \boldsymbol{F}_{el}^T) = \boldsymbol{\varepsilon_{el}} + \boldsymbol{\omega_{el}}$, in which $\boldsymbol{\varepsilon_{el}}$ accounts to pure deformation and $\boldsymbol{\omega_{el}}$ accounts to the rigid body rotation, according to the classical theory of elasticity results.

Since the mathematical formulation of the element is based on C_0 continuity shape functions, nodal components ε_k of a common node k connecting two or more elements may differ: nodal averaging of deformations by direct averaging their values at nodes has been introduced as an approximation. Calculation of approximate in-plane deformation inside each element was therefore performed by interpolating the averaged nodal values using the shape functions N_j as shown in Fig. 1c–e. The final loop in the FFNM method computes the approximate fiber deviation angle as the arctangent of the averaged "shear" strain as shown in Fig. 1 f: $\theta = \mathrm{ArcTan}(2\,\varepsilon_{xy})$.

2.3. Numerical and experimental methods for validation

The methodology was validated by micrograph analysis (Section 2.3.1) and mechanical testing (Section 2.3.2) techniques and a FEM model was built to exploit the potential of stiffness prediction (Section 2.3.3)

2.3.1. Optical Microscopy 2.3.1

The investigation of the method's capability and accuracy to detect local fiber orientation was done by extracting several CFRP specimens from each of the 3 manufactured plates, to allow capturing micrographs in at least 9 node locations on each plate and in at least 36 locations within each analyzed grid element. Wet ground with 400, 800, and 2500 grit SiC paper along fiber direction, as suggested by [13], was used to condition the specimens initially. Final polishing steps were performed using water-based alumina suspensions with progressively decreasing particle size. Particle size ranges were $3 \div 1$ μm in the first step, $0.5 \div 0.3$ μm in the further one. A low-napped silk polishing pad

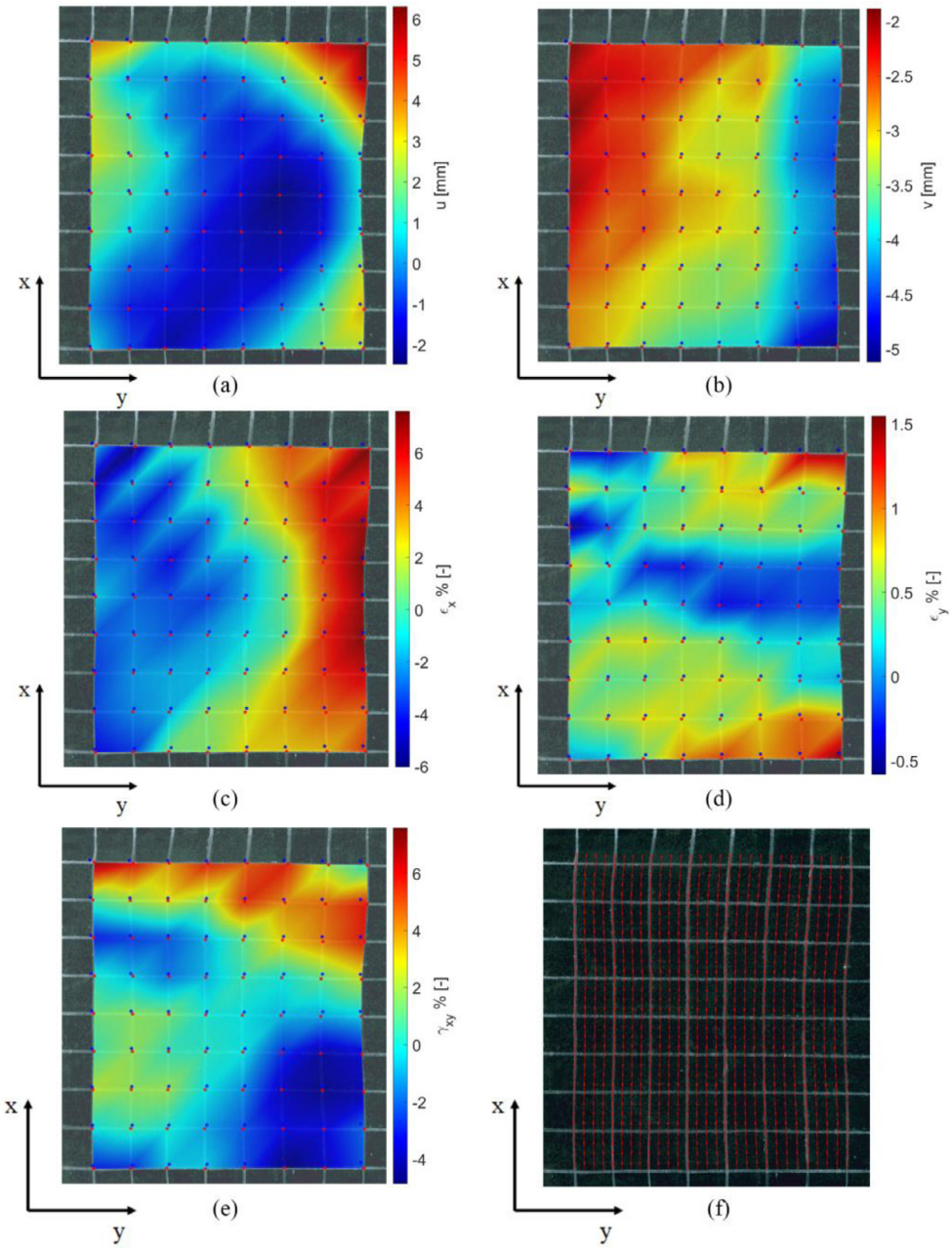

Fig. 1. Typical UD PCM plate analyzed with FFNM method utilizing 4 node element formulation. Blue Makers: corner location before compression molding. Red Markers: corner location after compression molding. a) u component of displacement. b) v component of displacement c) ϵ_x component of strain d) ϵ_y component of strain e) ϵ_{xy} component of strain f) Computed fiber orientation. (For interpretation of the references to color in this figure legend, the reader is referred to the web version of this article.)

was used for the alumina 3÷1 μm, while high-napped silk polishing for alumina 0.5÷0.3 μm. Samples were cleaned using an ultrasonic water bath after each polishing step and thus checked on an optical microscope to eliminate scratches induced by the previous step. Trials with dummy samples were conducted to optimize force, the platen's speed, and time to avoid fiber pullout and artifacts. Samples were studied using a Zeiss Axio Observer 3 at a magnification of 50x and acquired by an Infinity Lite B camera with a resolution of 1.5 megapixel, which results in a resolution of 2.5 μm/pixel. Micrographs were analyzed by the high-resolution misalignment analysis (HMRA) method [14] for its ability to be relatively insensitive to micrographic surface quality, by selecting a cell size of 80 μm for retrieving a stable standard deviation and by adopting a threshold for binarization of 0.45. Other useful parameters were: fiber diameter set to 7 μm (as measured on prepreg), minimum fiber diameter set to 3 μm, and minimum aspect ratio set to 6. The HMRA method measures fiber misalignment angles using a direct Matlab procedure, in which individual fibers are traced one at a time and measured on individual micrographs. Typical results for the adopted procedure are shown in Fig. 2, in which very few cells exhibit an overestimation of fiber deviation, as highlighted in Fig. 2 c. In these regions, individual fiber directions are not appropriately distinguished by the algorithm, contributing to an overall increase of the standard deviation. The spurious abnormous measurements, always located at the normal distribution tails, were mitigated by using the percentile filtering technique suggested by Wilhelmsson [20]. Detailed inspection on acquired micrographs suggested adopting 95:th percentile as a compromise between filtering of high spurious angles induced by the HMRA method and low filtering of real fiber waviness for the composite system studied herein.

2.3.2. *Mechanical testing 2.3.2*

Three tensile specimens were cut from each plate using a high-speed rotating diamond saw tool and checked for imperfections. Justification for the reduced number of ply was the maximization of the specimen's

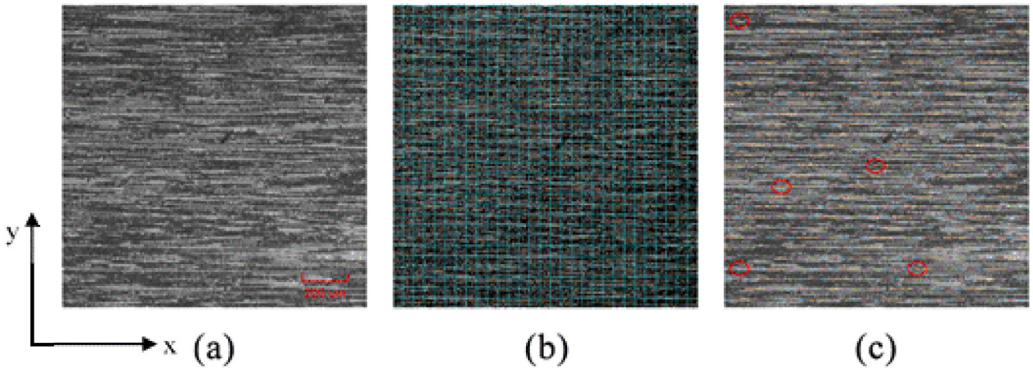

Fig. 2. Micrograph of a PCM UD sample prepared with the suggested procedure extracted from the top. a) original micrograph at 5x magnification. b) 80 μm cell decomposition c) post-processed micrograph by HMRA method with red circles highlighting cells with high deviation (spurious results). (For interpretation of the references to color in this figure legend, the reader is referred to the web version of this article.)

Table 1
Prepreg properties, P 384_S.

Properties	E_1 (GPa)	E_2 (GPa)	G_{12} (GPa)	ν_{12}
Value	115 ± 1	8.6 ± 0.46	4.4 ± 0.28	0.27 ± 0.016

frontal area (25 mm x 320 mm) while maintaining ultimate tensile force within compatible values for tabs and fixtures. A stochastic speckle pattern was applied on the front face using water-based paint: care was taken in optimizing the size and distribution of the pattern to ensure images were able to collect the wider possible region of each sample for the entire duration of the test. Tensile tests were carried out under displacement-controlled conditions at a constant cross-head rate of 2.5 mm/min into a servo-hydraulic INSTRON 8033 universal testing machine equipped with a 25 kN load cell. Specimens were monitored during tests at the frequency of 1 Hz by the two cameras of a 3D DIC system (Q-400, Dantec Dynamics, Skovlunde, Denmark), equipped with 17-mm lenses (Xenoplan, Schneider-Kreuznach, Bad Kreuznach, Germany). Istra-4D software (Dantec Dynamics) was employed to elaborate images and calculate displacements and strain distributions. Facet size and facet overlap were set to 25 pixels and 9 pixels, respectively, and a local regression displacement smoothing filter of 25 × 25 facets, available within Dantec software, was applied as a compromise between accuracy and spatial resolution according to [21]. Results were stored and exported to Matlab for further processing.

2.3.3. FEA Model 2.3.3

An additional analysis of the FFNM capability in predicting mechanical properties due to fiber misalignment was performed by modeling tensile specimens in Ansys APDL using solid elements (SOLID186). Element size was set to 0.8 mm as shown in Fig. 3-a, fiber misalignment angle was mapped and applied elementwise by rotating element coordinates systems as suggested by Wilhelmsson and others [22] and shown in Fig. 3 c.

Boundary forces and prescribed displacements were applied as nodal components on the corresponding surface of the mesh: bottom boundary was fixed in all degrees of freedom, the top boundary was fixed in the horizontal X direction of the model as shown in Fig. 3 b, and forces were introduced by dividing their values by node. Material data were self-measured according to applicable ASTM standards from autoclave processed plates and reported in Table 1.

3. Results and discussion

The misalignment angle measured over the 3 plates by the FFNM method is reported in Fig. 1. Regions from which tensile specimen were extracted is marked in black dashed line in both Fig. 4 a and c.

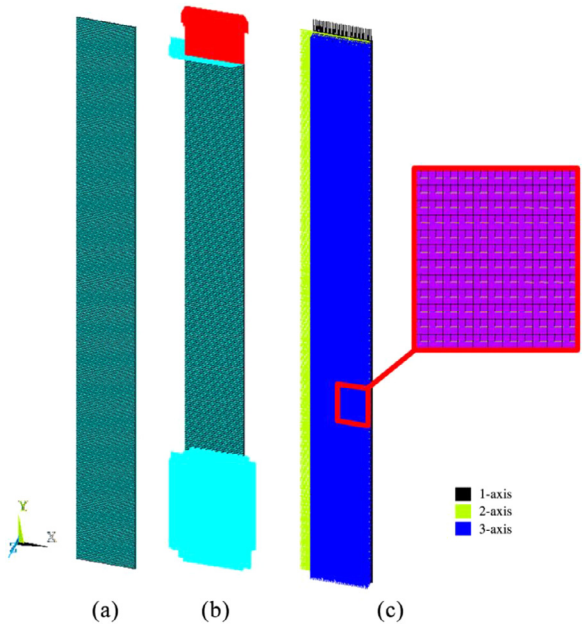

Fig. 3. FEA Model. a) mesh b) boundary conditions and forces c) coordinate element system.

3.1. Optical microscopy

The global accuracy of the FFNM method in detecting fiber misalignment is strictly related to its ability to correctly identify fiber misalignment at nodes, where the error on the displacement field is expected to approach a minimum. All plates in Fig. 4 show comparable misalignment angles in the range [-2°, 4°], with a sign that depends on the preferred direction of deformation of the grid. Plaques in Fig. 4 a and c show a moderate variation of misalignment between neighboring nodes for most of their extension whilst the plate of Fig. 4 b shows a more randomized misalignment in both nodes and elements. This peculiarity led to the decision to use the plaque of Fig. 4 b for a more extensive comparison with the HMRA method and to perform random checks on the nodes of the remaining slabs once the tensile specimens had been extracted.

To validate the approximations, discussed in Section 2.3.1, of strain averaging at nodes and interpolating averaged nodal values through polynomial shape functions, the investigation on the plaque of Fig. 4 b was performed within the representative inner region shown in Fig. 5. Fig. 6 compares the results of both FFNM and HMRA methods. The av-

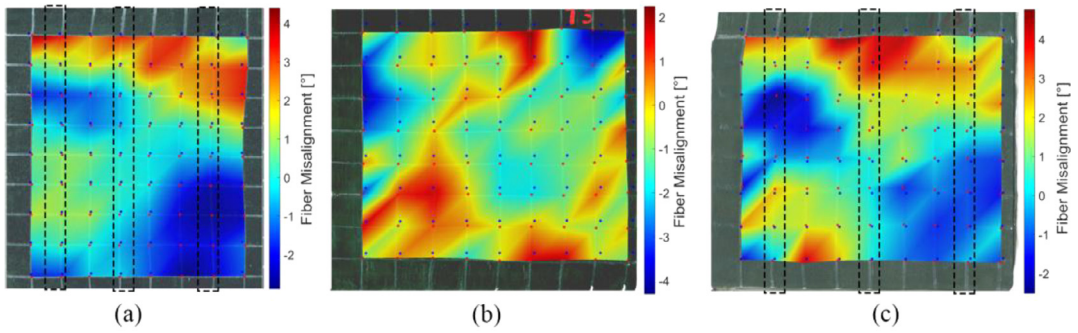

Fig. 4. Fiber misalignment detected on the 3 sample plates by FFNM method. Tensile specimen locations on molded plaques evidenced in black dashed line on a) and c)The accuracy of the method is experimentally benchmarked with the HMRA method and discussed in Section 3.1. Comparison of mechanical tests and FEA results are presented and discussed in Section 3.2.

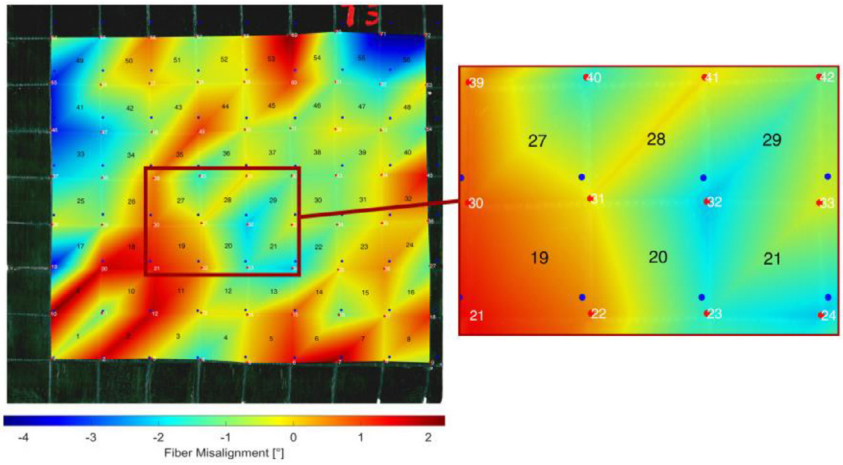

Fig. 5. Misalignment angle by the FFNM method and result in the representative inner region of the plate.

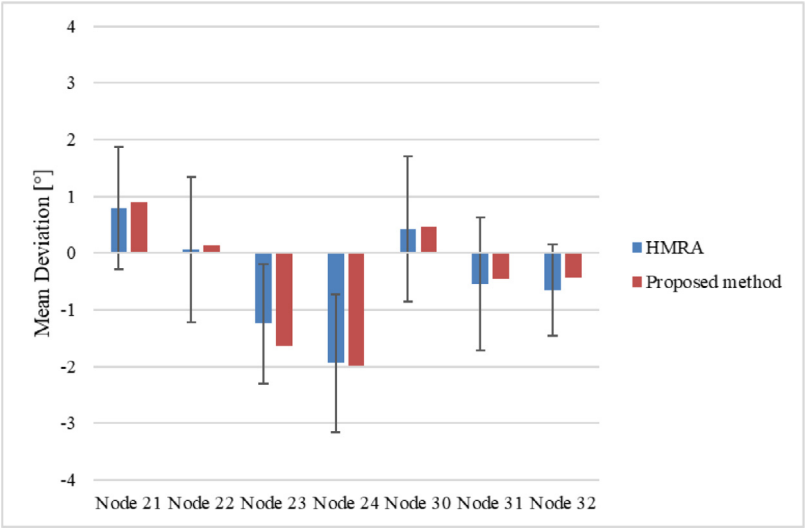

Fig. 6. Mean fiber orientation at different nodes evaluated by HMRA and present method using bilinear element formulation.

erage difference of the mean angle detected by the two methods was as small as 0.175°. Comparable results were obtained for samples extracted by the plates of Fig. 4 a and c. The HMRA method results reveal high standard deviation values, with a maximum value of 1.28°. The primary justification for these results can be related to the combination of (i) the contribution of the initial waviness of the prepreg, (ii) spurious measurements provided by the HMRA algorithm while processing micrographs with a high content of fibers, and (iii) additional misalignment caused by the friction between prepreg and the halves of the mold during processing. It is worth mentioning that the overall fiber deviation field reported in Fig. 1 f is not symmetric about the vertical axis of symmetry due to the high percentage of charge adopted in this study. Indeed, by analyzing the displacement field (Fig. 1 a and b), the flow appears to be highly anisotropic with a limited extension along the direction of the fibers.

This evidence highlight some potential limitation for the proposed methodology. Being the FFNM a surface technique, its precision in addressing fiber misalignment in internal plies is dependent on both flow

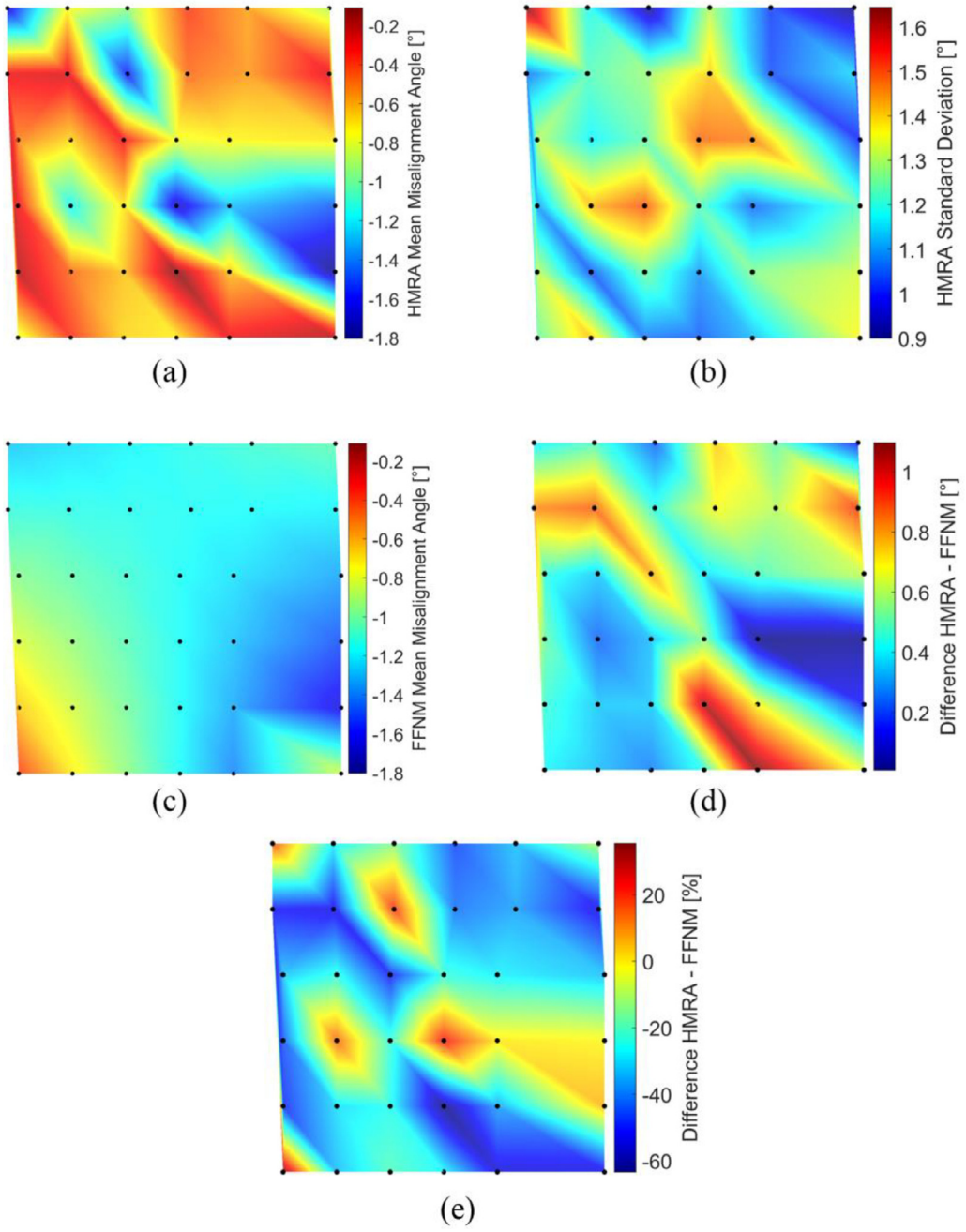

Fig. 7. Interpolated results of mean misalignment angle evaluated over a region. a)mean misalignment by HMRA method b) HMRA standard deviation c) misalignment angle by FFNM d) absolute difference between HMRA and FFNM.e) relative difference between HMRA and FFNM.

characteristics through the thickness of the laminate during processing and its stacking sequence. It can be argued that for laminates in which all plies are stacked with the same orientation and whenever the flow profile is constant through the thickness, measures of misalignment on external plies should be representative of the misalignment of the whole laminate. For stacking sequences having different orientations, measures from FFNM are strictly valid only on the surface of the component. This could be particularly useful for assessing flexural properties of PCM parts, where UD reinforcements are used in external plies to maximize bending stiffness and strength [23]. Interpolated results of comparing both FFNM and HMRA methods in a region about element 28 of Fig. 5 are presented in Fig. 7 to test the ability of shape function to represent the misalignment angle variation over an area correctly. Experimental measures of the mean misaligned angle over 36 sample micrographs, detected by the HMRA method and shown in Fig. 7 a, exhibits a non-linear distribution of angle variation, characterized as a random succession of local peaks and valleys. HMRA Standard deviation, depicted in Fig. 7 b, exhibits high values again compared to the mean misalignment measured angle. Interpolated results at sample points for the FFNM method are presented in Fig. 7 c in which angle variation appears to be bilinear as a consequence of the shape function formulation. Fig. 7 d shows the difference in measured angle by the two methods, where the highest values were is approached at one border. In this region, the lines of the grid drawn on the plate tend to become more curved, and linear interpolation can no longer adequately describe the displacement field of the plate's surface. From a detailed analysis of Fig. 7 d, in addition to the mentioned approximation error, the presence of random noise contained in a few tenths of a degree is observable. It

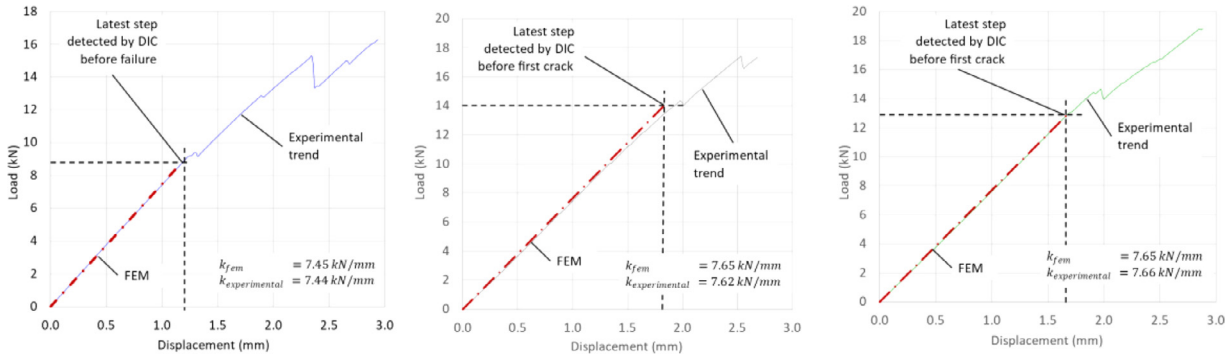

Fig. 8. Comparison of load versus displacement curves of the 3 different samples.

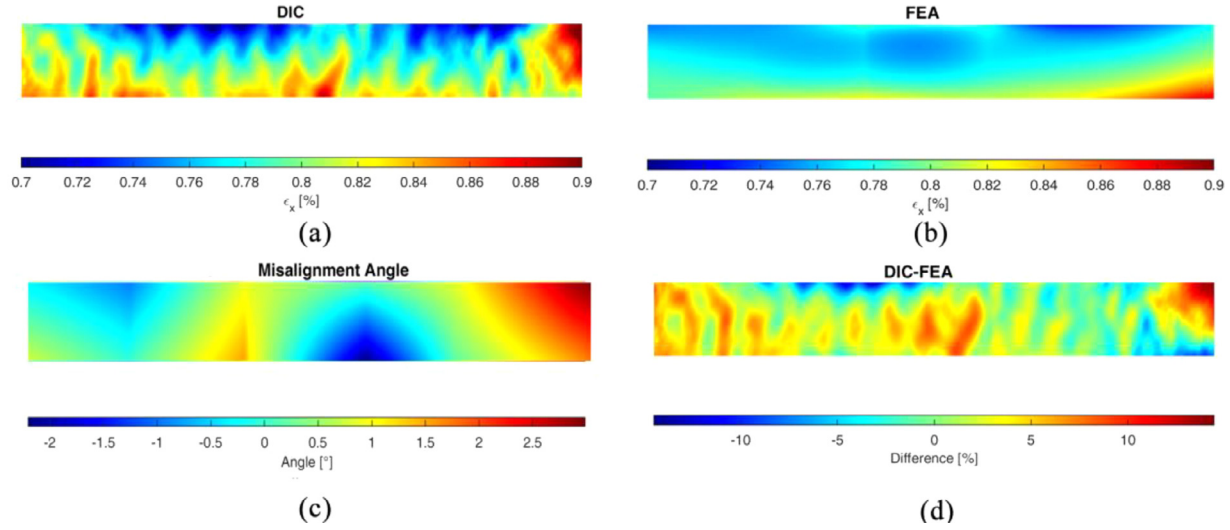

Fig. 9. Comparison between FEA analysis and DIC results on a typical sample. a) measured strain distribution by DIC system b) computed strain distribution by FE model c) contour p d) Difference between measured and computed strains.

can be argued that this effect may be caused partially by the local initial waviness of the prepreg which cannot be accounted for by the proposed method, whose scope is the evaluation of misalignment caused by processing.

For these reasons, a higher mean average difference of 0.5° was observed within the element, with a maximum of 1.1° in one micrograph over the bottom border of element 28. The relative difference between the two methods, calculated by the formula [24]

$$Relative\ Difference(\%) = 100 * \frac{\theta_{FFNM} - \theta_{statistical,\ HRMA}}{\min\left(\theta_{FFNM}, \theta_{statistical,\ HRMA}\right)} \quad (2)$$

is shown in Fig. 7 e. Note that the highest relative difference values were obtained for extremely small angles measured by HMRA (Fig. 7 a). This trend in relative difference could be partially explained by the limitations of interpolating by bilinear shape functions used in the proposed method, partially by the dependence of extracted fiber angle and pixel resolution by HRMA for very small misalignment angle [14], and partially on how the relative difference is calculated.

3.2. Mechanical test and FEA results

Comparison of tensile tests and FEA result of 3 representative samples are shown in Fig. 8, in which displacement was measured by the DIC system as the relative displacement of two gauge points positioned at the extrema of each sample. Experimental curves show several drops due to cracking of the laminate: progressive damage of each sample due to fiber misalignment was demonstrated by slope variation of force-displacement curves after each cracking. It is worth mentioning that depending on the position where specimens were cut from each plate, the tensile tests revealed different stiffness values. In particular, a maximum stiffness reduction of 4% concerning an aligned UD sample's stiffness was observed. Stiffness's values resulting from FEA, which included fiber orientation derived from the FFNM method, and calculated as the ratio k between applied loads and displacements at boundary nodes of the model, revealed a 1 % average mismatch to the experimental result.

These considerations support the FFNM method's effectiveness when used in combination with FEA to predict small local stiffness variations in the case of PCM composite components with misaligned long fibers.

Comparison between FEA strain results and DIC results are presented in Fig. 9. Results were evaluated at different applied loads and at the DIC system's latest steps within the linear region of each sample. First macroscopic failure on specimens occurred in those locations where the maximum absolute value of fiber deviation was detected. Indeed, these regions acted as a triggering point for through-thickness cracks that happened in the fiber-resin interface and the resin. As shown in Fig. 9-a, DIC results exhibit a non-uniform strain distribution on the surface, as a superimposition of local cracking of the laminate surface or noise [25] and effects due to misaligned fibers. Interestingly, strain distribution tends to become more uniform in the centerline of the specimen. A possible explanation is that due to in-plane bending introduced by fiber waviness, more considerable variations were mostly concentrated at borders, where matrix-dominated phenomena are more marked due to abrupt cut of fibers on edges. This phenomenon is partially confirmed

by the FFNM method's measurement and shown in Fig. 9 c: maximum values of strain measured by DIC were mainly located in regions where maximum misalignment was measured. Results from FEA, depicted in Fig. 9 b, predicted a more uniform strain distribution over the sample's surface. However, the difference between DIC and FEA results, shown in Fig. 8 d and evaluated as [(DIC strain) – (FEM strain)]/(DIC strain)x100, approaches a maximum mismatch value of about 15%. Maximum absolute difference was mainly located at the edges of each specimen, meaning that the linear FEM analysis was able to describe only an averaged representation of fiber misalignment induced effects.

4. Conclusion

A new, cost-effective and reliable methodology for fiber misalignment detection on PCM composites is presented in this work. A filtering algorithm has been developed to remove process-induced noise on images, thus extending the method's range of application. The approximate displacement field which occurred during compression molding was evaluated by interpolating the displacement of a set of sample points through polynomial interpolating functions. The fiber misalignment angle was successfully retrieved and benchmarked with one of the most recent and reliable methodologies available in the art state. Comparable results with even reduced standard deviation were obtained, proving the precision of the present method in measuring averaged fiber deviation in thin structures. The mechanical test has been performed on PCM samples, and for each sample, a FE model was developed by rotating elemental coordinate system according to fiber orientation estimated utilizing the new method. The experimental results showed that samples' stiffness could be predicted with great accuracy by the improved FE model. Strain distribution on the tensile samples' surface, captured immediately before their first macroscopic failure, was found to be highly inhomogeneous at borders due to matrix-dominated nonlinearities. In these regions, a maximum 15% strain error of the improved FEA model was detected. The technique will be used in the future using UV-visible ink to minimize the visual impact on manufactured parts and a general 3D formulation is under development for the analysis of in-plane fiber misalignment in curved components with complex shapes.

Declaration of Competing Interest

The authors declare that they have no known competing financial interests or personal relationships that could have appeared to influence the work reported in this paper.

Acknowledgment

The authors kindly acknowledge MIND Srl in Bologna, Italy, with a special thanks to G. Tagliaferri for his support in manufacturing the UD plates. A kindly acknowledge to Graduated Student Dr. Gabriele Sarti is given for his help in writing Matlab code.

Funding

This work was funded by Emilia Romagna region (Italy), Project name i-LBBox (CUP E31B19000230009).

Supplementary materials

Supplementary material associated with this article can be found, in the online version, at doi:10.1016/j.jcomc.2021.100151.

References

[1] M Pervaiz, S Panthapulakkal, B KC, M Sain, J Tjong, Emerging trends in automotive lightweighting through novel composite materials, Mater. Sci. Appl. (2016), doi:10.4236/msa.2016.71004.
[2] K. Akiyama, Development of preforming process in PCM (Prepreg Compression Molding) technology, 12th Annu Automot Compos Conf Exhib 2012 (ACCE 2012), 2013.
[3] DM Corbridge, LT Harper, DSA De Focatiis, NA. Warrior, Compression moulding of composites with hybrid fibre architectures, Compos. Part A (2017), doi:10.1016/j.compositesa.2016.12.018.
[4] D Bücheler, F. Henning, Hybrid resin improves position and alignment of continuously reinforced prepreg during compression co-molding with sheet molding compound, 17th Eur Conf Compos Mater, 2017.
[5] C Servais, A Luciani, JAE. Månson, Squeeze flow of concentrated long fibre suspensions: experiments and model, J. Nonnewton Fluid Mech. (2002), doi:10.1016/S0377-0257(02)00018-6.
[6] RB Pipes, DW Coffin, P Simacek, SF Shuler, RK. Okine, Rheological behavior of collimated fiber thermoplastic composite materials, Theor. Appl. Rheol. (1992), doi:10.1016/b978-0-444-89007-8.50390-7.
[7] J Mewis, AB. Metzner, The rheological properties of suspensions of fibres in Newtonian fluids subjected to extensional deformations, J. Fluid Mech. (1974), doi:10.1017/S0022112074000826.
[8] DE Sommer, AJ Favaloro, RB. Pipes, Coupling anisotropic viscosity and fiber orientation in applications to squeeze flow, J. Rheol. (2018), doi:10.1122/1.5013098.
[9] JY Shu, NA. Fleck, Microbuckle initiation in fibre composites under multiaxial loading, Proc. R. Soc. A Math. Phys. Eng. Sci. (1997), doi:10.1098/rspa.1997.0111.
[10] A Jumahat, C Soutis, FR Jones, A. Hodzic, Fracture mechanisms and failure analysis of carbon fibre/toughened epoxy composites subjected to compressive loading, Compos. Struct. (2010), doi:10.1016/j.compstruct.2009.08.010.
[11] Y Li, B Stier, B Bednarcyk, JW Simon, S. Reese, The effect of fiber misalignment on the homogenized properties of unidirectional fiber reinforced composites, Mech. Mater. (2016), doi:10.1016/j.mechmat.2015.10.002.
[12] SW. Yurgartis, Measurement of small angle fiber misalignments in continuous fiber composites, Compos. Sci. Technol. (1987), doi:10.1016/0266-3538(87)90016-9.
[13] K Kratmann, M Sutcliffe, L Lilleheden, R Pyrz, O Thomsen, A novel image analysis procedure for measuring fibre misalignment in unidirectional fibre composites, Compos. Sci. Technol. (2009) http://dx.doi.org/10.1016/j.compscitech.2008.10.020.
[14] D Wilhelmsson, LE. Asp, A high resolution method for characterisation of fibre misalignment angles in composites, Compos. Sci. Technol. (2018), doi:10.1016/j.compscitech.2018.07.002.
[15] NQ Nguyen, M Mehdikhani, I Straumit, L Gorbatikh, L Lessard, SV Lomov, Micro-CT measurement of fibre misalignment: application to carbon/epoxy laminates manufactured in autoclave and by vacuum assisted resin transfer moulding, Compos. Part A (2018), doi:10.1016/j.compositesa.2017.10.018.
[16] K Mizukami, Y Mizutani, A Todoroki, Y. Suzuki, Detection of in-plane and out-of-plane fiber waviness in unidirectional carbon fiber reinforced composites using eddy current testing, Compos. Part B (2016), doi:10.1016/j.compositesb.2015.09.041.
[17] RR Cook, DS Malkus, ME Pelsha, RJ. Witt, Concepts and Applications of Finite Element Analysis, John Wiley Sons Inc, 2002.
[18] V Griffiths D, Stiffness matrix of the four?node quadrilateral element in closed form, Int. J. Numer. Methods Eng. (1994), doi:10.1002/nme.1620370609.
[19] W Buerzle, E. Mazza, On the deformation behavior of human amnion, J. Biomech. (2013), doi:10.1016/j.jbiomech.2013.05.018.
[20] D Wilhelmsson, R Gutkin, F Edgren, LE. Asp, An experimental study of fibre waviness and its effects on compressive properties of unidirectional NCF composites, Compos. Part A (2018), doi:10.1016/j.compositesa.2018.02.013.
[21] M Palanca, TM Brugo, L Cristofolini, Use of digital image correlation to investigate the biomechanics of the vertebra, J. Mech. Med. Biol. (2015), doi:10.1142/s0219519415400047.
[22] D Wilhelmsson, LE Asp, R Gutkin, F. Edgren, Fibre waviness induced bending in compression tests of uniderectional NCF composites, ICCM Int Conf Compos Mater, 2017 Volume 201.
[23] DM Corbridge, LT Harper, DSA De Focatiis, NA. Warrior, Compression moulding of composites with hybrid fibre architectures, Compos. Part A (2017), doi:10.1016/j.compositesa.2016.12.018.
[24] L Törnqvist, P Vartia, YO. Vartia, How should relative changes be measured? Am. Stat. (1985), doi:10.1080/00031305.1985.10479385.
[25] LF Sánchez-Heres, JW Ringsberg, E Johnson, Characterization of non-crimp fabric laminates: loss of accuracy due to strain measuring techniques, J. Test. Eval. (2016), doi:10.1520/jte20150051.